Published in final edited form as:
Cancer Res. 2012 April 1; 72(7): 1878–1889. doi:10.1158/0008-5472.CAN-11-3132.

*Pten*loss and RAS/MAPK activation cooperate to promote EMT and metastasis initiated from prostate cancer stem/progenitor cells

David J Mulholland[1], **Naoko Kobayashi**[1], **Marcus Ruscetti**[1], **Allen Zhi**[1], **Linh M Tran**[1], **Jiaoti Huang**[2], **Martin Gleave**[3], and **Hong Wu**[1,4,*]

[1]Department of Molecular and Medical Pharmacology and Institute for Molecular Medicine

[2]Department of Pathology and Laboratory Medicine, David Geffen School of Medicine, University of California Los Angeles

[3]The Vancouver Prostate Centre and University of British Columbia, Vancouver, BC

[4]Eli and Edythe Broad Center of Regenerative Medicine and Stem Cell Research, University of California, Los Angeles

Abstract

PTEN loss or PI3K/AKT signaling pathway activation correlates with human prostate cancer progression and metastasis. However, in preclinical murine models, deletion of *Pten* alone fails to mimic the significant metastatic burden that frequently accompanies the end stage of human disease. To identify additional pathway alterations that cooperate with PTEN loss in prostate cancer progression, we surveyed human prostate cancer tissue microarrays and found that the RAS/MAPK pathway is significantly elevated both in primary and metastatic lesions. In an attempt to model this event, we crossed conditional activatable *K-ras*$^{G12D/WT}$ mice with the prostate conditional *Pten* deletion model. Although RAS activation alone cannot initiate prostate cancer development, it significantly accelerated progression caused by PTEN loss, accompanied by epithelial-to-mesenchymal transition (EMT) and macrometastasis with 100% penetrance. A novel stem/progenitor subpopulation with mesenchymal characteristics was isolated from the compound mutant prostates, which was highly metastatic upon orthotopic transplantation. Importantly, inhibition of RAS/MAPK signaling by PD325901, a MEK inhibitor, significantly reduced the metastatic progression initiated from transplanted stem/progenitor cells. Collectively, our findings indicate that activation of RAS/MAPK signaling serves as a potentiating second hit to alteration of the PTEN/PI3K/AKT axis and co-targeting both pathways is highly effective gin preventing the development of metastatic prostate cancers.

INTRODUCTION

Prostate cancer is the most common male malignancy and a frequent cause of mortality in western countries (1). During late stage disease, oncogenic signaling pathways act collaboratively to promote metastasis and castration resistant prostate cancer (CRPC) development. Alteration of the PTEN/PI3K/AKT pathway is well correlated with prostate cancer development with about 70% of late stage samples showing PTEN loss or PI3K activation (2). The *Pten*-null prostate cancer model mimics human disease including hyperplasia, PIN and invasive carcinoma with defined kinetics (3). However, inactivation of

*Corresponding author: Hong Wu, M.D, Ph.D., CHS 33-131E, 650 Charles E Young Drive S., Los Angeles, CA 90095, Phone: 310.825.5160, FAX: 310.267.0242, hwu@mednet.ucla.edu .

Pten alone (3) (4) (5) or in combination with homozygous deletion of p53 (6) (7) or Nkx3.1 (8) fails to recapitulate the critical aspect of end stage human prostate cancer, i.e., significant metastatic burden. Thus, identification of signaling mechanisms that collaborate with alteration of the PI3K pathway in promoting prostate cancer metastasis is critical for modeling late stage of human disease and for testing therapeutic strategies.

Despite the low frequencies of RAS mutations (9-11) (12) and RAS fusion events (13), compelling evidence suggests that RAS/MAPK pathway activation plays a significant role in human prostate cancer progression, particularly in metastasis and CRPC development. Enhanced *RAS* signaling can reduce dependency for androgens in the LNCaP prostate cancer cell line (14), while inhibition of RAS can restore hormone dependence in C42 cells, a line that is otherwise hormone independent (14) (15). Further, patients who have failed hormone ablation therapy display augmentation of P-MAPK levels, a downstream target of RAS signaling (16). Finally, RAS activation in the DU145 human prostate cancer cell line can promote metastasis to the brain and bone (17). Despite these in vitro observations, it is unclear 1) whether activation of the RAS/MAPK pathway is sufficient to initiate the full spectrum of prostate cancer development and 2) whether the RAS/MAPK pathway can collaborate with the PTEN/PI3K pathway in promoting metastasis and CRPC development.

We hypothesized that activating the RAS/MAPK pathway in conjunction with reduced *Pten* dosage may promote metastasis. To test this hypothesis, we incorporated the activating *K-ras*$^{G12D/WT}$ allele (18), as a means to activate the RAS/MAPK axis, to the *Pten*-null prostate cancer model that we generated previously (3). We report here the important collaborative effects of RAS/MAPK and PTEN/PI3K pathways in promoting prostate cancer metastasis and potential molecular mechanisms underlying such collaboration. Collectively, our results suggest that RAS/MAPK pathway activation may serve as a critical “second hit” to PTEN/PI3K/AKT pathway alterations to androgen dependent prostate cancer and CRPC.

METHODS

Human TMA and bone metastasis samples

Human prostate cancer tissue microarrays (TMA) are composed of 194 patients and 388 cores (19). Histopathological composition of the array is outlined in Supplemental Figure 1. All bone metastasis are from prostate cancer patients with abnormal bone scans.

Mouse strains, tissue collection and reconstitution

Mutant mice with prostate specific deletion of *Pten* were generated as previously described under a mixed background (3). To generate the *Pb-Cre*$^{+}$*;Pten*$^{L/L}$*;K-ras*$^{G12D/W}$ or *Pb-Cre*$^{+}$*;Pten*$^{L/W}$*;K-ras*$^{G12D/W}$ mice, *Pb-Cre*$^{+}$*;Pten*$^{L/W}$ male mice were bred with female *Cre*$^{-}$*;Pten*$^{L/L}$*;K-ras*$^{G12D/W}$ mice (20). To generate *Pb-Cre*$^{+}$*;Pten*$^{L/L}$*;K-ras*$^{G12D/W}$*;LSL-Rosa26-LacZ* or *Pb-Cre*$^{+}$*;Pten*$^{L/L}$*;K-ras*$^{G12D/W}$*;LSL-Rosa26-Luc* mice, *Cre*$^{+}$*;Pten*$^{L/L}$*;K-ras*$^{G12D/W}$ male mice were bred with female, *Cre*$^{-}$*; Pten*$^{L/L}$*;LSL-Rosa26-LacZ* (21) or *Cre*$^{-}$*; Pten*$^{L/L}$*;LSL-Rosa26-Luc* (*LSL-Rosa26-Luc* was obtained from NCI eMICE Strain 01XAC). All animal housing, breeding and surgical procedures were performed under the regulation of the Division of Laboratory Animal Medicine at the University of California at Los Angeles.

mRNA Extraction and Microarray Hybridization

RNA was extracted from pooled lobes resected from mutant prostates. Microarrays were performed in the UCLA Clinical Microarray Facility using Affymetrix mouse 430 2 arrays. In brief, total RNA was extracted using the miRNeasy Mini Kit (Qiagen). Array hybridization, washing, and scanning were carried out as per the manufacturer’s

instructions. For genes represented by multiple probes, its expression was represented by the average of its probe expressions. Microarray data are available at the National Center for Biotechnology Information Gene Expression Omnibus (GSE34839).

Rank-Rank Analysis

In rank-rank geometric overlap analysis (RRHO) genes in human data sets derived from Lapointe et al. (22) and Taylor et al., (2) were ranked based on their log-transformed p-values of t-test comparing between two subgroups/genotypes as previously described (23) (24).

Immunohistochemistry and LacZ detection

To detect LacZ+ cells, frozen sections were fixed in methanol, followed by X-gal staining (25) for 6-12 hours and then counterstained with fast red. Immunohistochemistry was carried out as previously described (3) (26) using the following antibodies: PTEN (Cell Sig., 9559), P-MAPK (Cell Sig., 4376), AR (Santa Cruz, sc-816), Pan-cytokeratin (Sigma, C1801), E-cadherin (Cell Sig., 610181), Vimentin (Abcam, ab39376), P-AKT (Cell Sig., 3787), Ki67 (Vector, VP-RM04), p63 (BD transduction, 559952).

FACS analysis and cell sorting

Cell isolation was carried out as previously described (26) using the following FACS antibodies: Sca1-PE (BD Pharm, 553336), CD49f-APC (Biolegend, 313610), Epcam-APC/Cy7 (Biolegend, 118218), CD24-PE/Cy7 (Biolegend, 101822).

RT-PCR

Total RNA was extracted from the mouse prostate or from the sorted cells using TRIzol reagent (Invitrogen) and purified using an RNeasy Mini column (Qiagen) according to the manufacturers' protocols. One microgram of purified total RNA was reverse transcribed to cDNA by the High-Prostate canceracity cDNA Archive Kit (Applied Biosystems: Foster City, CA, USA) with the random primers and MultiScribe Reverse Transcriptase. The relative gene expressions were measured by real-time RT-PCR using the gene-specific primers and iQ™ SYBR^{R} Green Supermix (Bio-Rad) compared to the RPL13a RNA quantity for each cDNA sample as an endogenous control. Primers used for cell lineage marker expression were used as previously described (27) and EMT markers as follows: *Cdh1*(F) (CAGGTCTCCTCATGGCTTTGC), *Cdh1* (R) (CTTCCGAAAAGAAGGCTGTCC); *Fn* (F) (AGCAGTGGGAACGGACCTAC), *Fn* (R) (ACGTAGGACGTCCCAGCAGC); *Foxc2* (F) (AAGATCACTCTGAACGGCATC), *Foxc2* (R) (CACTTTCACGAAGCACTCATTG); *Mmp2* (F) (CACCTACACCAAGAACTTCC), *Mmp2* (R) (GAACACAGCCTTCTCCTCCT); *N-cad* (F) (CAGGTCTCCTCATGGCTTTGC), *N-cad* (R) (CTTCCGAAAAGAAGGCTGTCC); *RPL13a* (F) (TACGCTGTGAAGGCATCAAC), *RPL13b* (R) (ATCCCATCCAACACCTTGAG); *Snai1* (F) (AAGATGCACATCCGAAGC), *Snai1* (R) (ATCTCTTCACATCCGAGTGG); Twist (F) (CGGGTCATGGCTAACGTG), Twist (R) (CAGCTTGCCATCTTGGAGTC); *Vim* (F) (CGGCTGCGAGAGAAATTGC), *Vim* (R) (CCACTTTCCGTTCAAGGTCAAG); Zeb1 (F) (CATGTGACCTGTGTGACAAG), *Zeb1* (R) (GCGGTGATTCATGTGTTGAG); Zeb2 (F) (TAGCCGGTCCAGAAGAAATG), *Zeb2* (R) (GGCCATCTCTTTCCTCCAGT).

Cell line

The *Pten*$^{-/-}$;*Kras*^{G12D} cell line was isolated from a 10 wk *C*$^{+}$;*Pten*$^{L/L}$;*K-ras*$^{L/W}$ mutant prostate through FACS sorting of Lin^{-}Epcam^{high}CD24^{high} cells. Cells were passaged in culture at least 10 times and PCR authenticated for *Pten* deletion and the presence of the *K-*

ras^{G12D} activating allele. *Pten*$^{-/-}$;*Kras*^{G12D} cells were infected with lenti GFP virus for detection by immunohistochemistry.

Orthotopic injections, bioluminescence imaging and measurement of lung lesions

Prostate sphere cells or subpopulations of primary cancer cells were isolated from *C*$^{+}$;*Pten*$^{L/L}$;*K-ras*$^{L/W}$;*LSL-Luc* mutant prostates. Prostate orthotopic injections were carried out using approximately 2000 cells in 50% matrigel/media using a 10 ul Hamilton syringe (Microliter #701). Tumor development was then monitored using bioluminescence detection (Xenogen IVIS, Caliper Life Sciences). For measurement of lung lesions, accumulated lesion area per mouse was measured and then calculated as a percentage of total lung section area. Tibial, orthotopic injections to *NOD;SCID;IL2rγ*-null recipients were carried out using an 10 ul Hamilton syringe (Microliter #701) to deliver no more 1000 *Pten*$^{-/-}$;*Kras*^{G12D} cells injected in 10 ul volume of 50% Matrigel/Media.

Drug treatment

NOD;SCID;IL2rγ-null mice with various orthotopic transplantations were treated with rapamycin (4 mg/kg/d, I.P) and/or PD325901 (10 mg/kg/d, P.O.) daily for 14 days.

RESULTS

RAS/MAPK pathway is activated in human primary and metastatic prostate cancer lesions

Of several well known pathways alterations found in human prostate cancers is the RAS/RAF/MAPK pathway, showing frequencies of 43% and 90% alteration in primary and metastatic lesions, respectively (2). To investigate the potential collaboration between the PTEN/PI3K and RAS/MAPK pathways, we assessed the correlation between PTEN loss and MAPK activation using: 1) a human prostate cancer tissue microarray (TMA) composed of 194 patients and 388 cores (Fig. 1A and Supplementary Fig. 1) and 2) thirty human prostate cancer bone metastasis specimens obtained from 4 U.S. medical institutions (Fig. 1B). While P-MAPK levels were not significantly elevated in untreated specimens, levels were significantly increased in neoadjuvant treated (NHT), recurrent and CRPC patients as compared to benign prostatic hyperplasia (BPH) specimens, coinciding with at least a 1-fold reduction in PTEN expression (Fig. 1A, *, $p<0.05$; **, $p<0.005$). In metastatic bone lesions, we observed elevated P-MAPK staining in 80% (24/30) of samples (Fig. 1B), a finding similar to what was reported previously for lymph node metastasis (28). In nearly all bone lesions, PTEN expression was low or negative (Fig. 1B; right panel). Interestingly, prominent P-MAPK expression was found near the basal compartment, corresponding to the potential transient amplifying stem/progenitor cell populations in human bone metastatic lesions (Fig. 1B; arrow). Collectively, these data indicate that the RAS/MAPK signaling pathway is highly active in human prostate cancer specifically in patients who have received anti-androgen therapy. These data also suggest that there may be selection for coinciding activation of PI3K/AKT and RAS/MAPK signaling in patients with late stage disease.

PTEN loss and RAS activation cooperate in accelerating primary and metastatic prostate cancer progression

To assess the role of RAS pathway activation in promoting prostate cancer development and metastasis we conditionally activated *K-ras* in the prostatic epithelium by crossing the *K-ras*$^{G12D/W}$ (*K-ras*$^{L/W}$) (29) allele to the *Pb-Cre* line (*C*$^{+}$) (30). While RAS activation was sufficient to enhance P-MAPK levels, it failed to promote significant cell proliferation, AKT activation and prostate cancer development (Supplemental Fig 2). Therefore, activation of the RAS pathway alone is not sufficient to induce prostate cancer. To assess RAS/MAPK activation as an additional hit to PTEN/PI3K/AKT pathway alteration in promoting prostate

cancer progression, we crossed *Pb-Cre*$^{+}$*;Pten*$^{L/L}$ mice (*C*$^{+}$*;Pten*$^{L/L}$) with *K-ras*$^{L/W}$ mice to generate *C*$^{+}$*;Pten*$^{L/L}$*;K-ras*$^{L/W}$ mutants. In comparison to *C*$^{+}$*;Pten*$^{L/L}$ mutants, simultaneously deleting *Pten* and activating *K-ras* led to early lethality (Fig. 1A, comparing red and green lines) with enhanced progression at both gross (Fig. 2B; arrows, anterior lobes; arrow heads, dorsolateral lobes) and histological levels (Fig. 2C). While pathology in *C*$^{+}$*;Pten*$^{L/L}$ mutants was predominantly adenocarcinoma localized to the dorsal-lateral lobes, *C*$^{+}$*;Pten*$^{L/L}$*;K-ras*$^{L/W}$ mutants showed invasive carcinoma both in the dorsal-lateral and anterior lobes as early as 4 weeks with poorly differentiated carcinoma occurring by 10 weeks (Fig. 2B, C).

Since partially reduced PTEN expression occurs frequently during human prostate cancer progression (Fig 1B) (31, 32), we then considered whether loss of a single *Pten* allele could also cooperate with RAS activation. While under the genetic background we studied, neither *C*$^{+}$*;Pten*$^{L/WT}$ (3) (26) (24) or *C*$^{+}$*;K-ras*$^{L/WT}$ mutants showed little evidence of cancer when aged to more than 1 year (data not shown and Supplemental Fig. 2), *C*$^{+}$*;Pten*$^{L/W}$*;K-ras*$^{L/W}$ mice developed focal neoplastic expansions by 10 weeks, invasive carcinoma by 20 weeks (Supplemental Fig. 4A, B) and lethality around 40 weeks (Fig. 2A, orange line) accompanied by PTEN loss and P-AKT-S473 activation (Supplemental Fig. 4C).

Importantly, in contrast to micrometastasis seen in 15-30% of age- and genetic background-matched *C*$^{+}$*;Pten*$^{L/L}$ mice (3), both *C*$^{+}$*;Pten*$^{L/L}$*;K-ras*$^{L/W}$ and *C*$^{+}$*;Pten*$^{L/W}$*;K-ras*$^{L/W}$ mutants developed macrometastatic lesions in the lung and liver with 100% penetrance (Fig. 3A). Lesions were largely pan-cytokeratin positive (Fig. 3A) with activated MAPK and PTEN loss (Fig. 3B). Interestingly, AR expression was highly heterogeneous in lung lesions (Fig 3A) and primary tumor samples from *C*$^{+}$*;Pten*$^{L/W}$*;K-ras*$^{L/W}$ mutants (Supplemental Fig 3A). Moreover, Gene Set Enrichment Analysis (GSEA) demonstrated that *C*$^{+}$*;Pten*$^{L/L}$*;K-ras*$^{L/W}$ mutant prostates have reduced expression of AR target genes (Supplemental Fig 3C), in comparison to *C*$^{+}$*;Pten*$^{L/L}$ mutants, including *Mme, Msmb* and *Nkx3.1* (Supplemental Fig 3C).

Importantly, cells with genotype of Cre^{+}, *Pten* deletion and activated *K-ras* were detected in 4/6 bone marrow flushes of *C*$^{+}$*;Pten*$^{L/L}$*;K-ras*$^{L/W}$ or *C*$^{+}$*;Pten*$^{L/W}$*;K-ras*$^{L/W}$ mutants (Fig. 3C). However, due to early lethality of these animals, we did not observe overt metastasis to the bone at the histological level or by bone image (data not shown). Collectively, our results indicate that the cooperation between PTEN loss and RAS activation yields significantly enhanced metastatic prostate cancer progression in these new murine models.

RAS activation promotes *Pten* null epithelial cells to undergo EMT and acquisition of a human prostate cancer signature

A striking feature found in *C*$^{+}$*;Pten*$^{L/L}$*;K-ras*$^{L/W}$ and *C*$^{+}$*;Pten*$^{L/W}$*;K-ras*$^{L/W}$ prostates was the mesenchymal morphology associated with the aggressive behavior of cancer cells, similar to poorly differentiated human cancers (Supplemental Fig 5). Similar to human prostate cancer, we observed a loss of p63 expression in the basal compartment of cancerous acini of *C*$^{+}$*;Pten*$^{L/L}$*;K-ras*$^{L/W}$ mutants (Supplemental Fig 5A). We also observed further reduction of p53 and p27 in *C*$^{+}$*;Pten*$^{L/L}$*;K-ras*$^{L/W}$ mutants compared to those with *Pten* single deletion (Supplemental Fig 5B). Consistent with EMT phenotype, we observed enhanced N-cadherin expression in transition regions, especially in poorly differentiated cancer, indicating that many of these cells displayed neuroendocrine expansion. Interestingly, synaptophysin positive cells were generally rare in this new model (Supplemental Fig 5C).

To assess the role of Ras activation in promoting epithelial-to-mesenchymal transition (EMT) in *Pten* null epithelium, we examined regions with morphological transition using the epithelial (E-cadherin) and mesenchymal markers (Vimentin) (Fig. 4A). While

adenocarcinoma and mesenchymal cancer regions showed distinct marker expression, transition regions showed coexpression of both epithelial and mesenchymal markers (Fig. 4A; yellow in overlay).

To ascertain that the observed mesenchymal pathology occurred as a result of a true EMT, and not expansion of the native stromal compartment, we crossed a Cre-activatable *Lac-Z* reporter line (*LSL-Rosa26-LacZ*) (25) onto the compound mutant line. Since *Lac-Z* expression is activated by the same Cre recombinase, LacZ+ cells could be used for lineage tracing for those *Pten* null and *Ras* activated epithelial cells. Analysis of $C^{+};Pten^{L/L};$*LSL-Rosa26-Lac-Z* mutant prostates showed LacZ positive regions to be restricted to prostate epithelium (data not shown); however, $C^{+};Pten^{L/L};K\text{-}ras^{L/W};$*LSL-Rosa26-LacZ* prostates showed expansion of *Lac-Z* positive cells from epithelial acini (arrows Fig. 4B) to regions with mesenchymal morphology (arrowheads in Fig. 4B, center panel). These data indicate that RAS activation facilitates EMT of *Pten* null epithelial cells.

We then conducted unbiased microarray analysis on age- and genetic background-matched $C^{+};Pten^{L/L};K\text{-}ras^{L/W}$ and $C^{+};Pten^{L/L}$ prostates (n=3; 10 wks) and found that 370 and 336 genes were significantly up and down regulated for more than 3-fold, respectively, due to RAS activation. Among those up-regulated genes, 11 were EMT-associated genes (p = 1.7e-13, Fisher's exact test) (Fig. 4C). We further validated the array analysis by real time PCR using independent prostate samples from $C^{+};K\text{-}ras^{L/W}$, $C^{+};Pten^{L/L}$ and $C^{+};Pten^{L/L};K\text{-}ras^{L/W}$ mutants at 10 week of age. Prostates from $C^{+};Pten^{L/L};K\text{-}ras^{L/W}$ mutants showed significantly enhanced expression of EMT markers including Snail (*Snai1*), Vimentin (*Vim*), Fibronectin (*Fn1*), MMP2 (*Mmp2*), Twist (*Twist1*), Zeb1 (*Zeb1*) and Foxc2 (*Foxc2*) (Fig. 4D). Thus, at the gene expression level, $C^{+};Pten^{L/L};K\text{-}ras^{L/W}$ mutants display an EMT signature.

Because of the association of PTEN/PI3K/AKT and RAS/RAF/MAPK pathway alterations in human prostate cancer progression, we hypothesized that murine prostate cancer with concomitant PTEN and RAS pathway alterations may closely resemble gene signatures of end stage human prostate cancers. To test this hypothesis, we used Rank-Rank (RRHO) analysis to compare the overlap of differentially expressed genes in human primary vs. metastatic tumors from either the Lapointe et al. (22) or Taylor et al. (2) data sets with either $Pb\text{-}C^{+};Pten^{L/L}$ or $Pb\text{-}C^{+};Pten^{L/L};K\text{-}ras^{L/W}$ mutants. The heat map signals on the bottom left (blue circle) and top right (red circle) corners indicate that primary human tumors shared the greatest overlap with $Pb\text{-}C^{+};Pten^{L/L}$ primary tumors while the human metastatic data set overlapped more with the signature derived from $Pb\text{-}C^{+};Pten^{L/L};K\text{-}ras^{L/W}$ mutants (Supplemental Fig 6A).

Based on previously published RAS signature gene sets (33), several were noted to be altered to a greater extent in *Pten;K-ras* metastatic lesions, similar to that of human disease, as exemplified by the down regulation of *FGFR2* expression and enhanced *UBE2C* expression, a ubiquitin conjugating enzyme known to be over expressed in human Prostate cancer (Supplemental Fig 6B) (34). Together, these analyses provide strong support of our hypothesis that the *Pten;K-ras* model closely mimics the biology of human prostate cancer, especially metastatic disease.

Pten loss and Ras activation cooperate to enhance stem/progenitor activity

Recent studies suggest that EMT is associated with the formation of breast cancer stem cells (35) and the progression of prostate cancer (19, 36). To test whether RAS activation induces EMT in *Pten* null prostatic stem/progenitor cells and consequently promotes prostate cancer progression and metastasis, we characterized prostatic stem/progenitor cells in vitro sphere forming analysis. Our previous study indicates that LSC^{high} ($Lin^{-}Sca1^{+}CD49f^{high}$) stem/

progenitor cells have high sphere-forming activity and are both necessary and sufficient for initiating *Pten* null prostate cancers (26). Similar to *Pten* null prostates, the compound *Pten*;*K-ras* prostates showed significant expansion of the LSC^{high} subpopulation (Fig. 5A, left panel; **, $p<0.01$, n=4) and further enhanced sphere forming activity (Fig. 5A, right panel, **, $p<0.01$). However, different from *Pten* null prostates, the LSC^{low} ($Lin^{-}Sca1^{+}CD49f^{low}$) subpopulation isolated from the compound mutants had significantly enhanced sphere forming activity in free floating conditions (Fig. 5A, right panel; *, $p<0.05$). To assess whether certain epithelial stem/progenitor cells have acquired mesenchymal characteristics and, therefore, reduced epithelial marker expression on the cell surface, we isolated $Lin^{-}Epcam^{low}CD24^{low}$ cells from the above mutants and found that only $Lin^{-}Epcam^{low}CD24^{low}$ cells (Fig 5B, right FACS plot) from $C^{+};Pten^{L/L};K\text{-}ras^{L/W}$ mutants had significant sphere forming activity ($p<0.001$; Fig. 5A, right panel). Using real time PCR analysis, we affirmed that LSC^{high} and LSC^{low} subpopulations corresponded to the basal (*Ck5, p63, Ck14*), and luminal cell populations (*Ar, Ck8, Ck18, E-cdh* and *Psca*), respectively, while the $Epcam^{low}/CD24^{low}$ subpopulation corresponded to mesenchymal cells based on the heightened gene expression of *Ar, Mmp2, N-cadherin, Snail, Twist, Vimentin* and *Zeb2* (Fig. 5B; n=4). Therefore, *Pten* loss and *Ras* activation collaborate in stem/progenitor expansion and Ras activation promotes EMT in *Pten* null sphere-forming cells.

Stem/progenitor cells with Pten loss and Ras activation can reconstitute EMT and macrometastatic prostate cancer

Our previous study demonstrated that the LSC^{high} subpopulation or its derived sphere cells isolated from *Pten* null primary cancers could reconstitute adenocarcinoma when subject to the prostate regeneration assay (26). Since primary $C^{+};Pten^{L/L};K\text{-}ras^{L/W}$ mutants develop macrometastasis, we then considered whether sphere cells derived from these mutants could also initiate a metastatic phenotype via orthotopic transplantations, an assay thought to closely mimic the natural metastatic process (37). To test this, we dissociated passage 3 sphere cells from $C^{+};K\text{-}ras^{L/W}$, $C^{+};Pten^{L/L}$ and $C^{+};Pten^{L/L};K\text{-}ras^{L/W}$ mice followed by orthotopic injection of approximately 2×10^{3} cells to the proximal region of the anterior lobe of *NOD;SCID;IL2rg*-null mice. Genotypes of sphere cells were confirmed by PCR analysis, prior to transplantation, on individual P3 spheres (Supplemental Fig. 7A and data not shown).

Although $C^{+};Pten^{L/L}$ (data not shown) and $C^{+};Pten^{L/L};K\text{-}ras^{L/W}$ sphere cells could initiate primary engraftments after 3-4 weeks, only recipient mice with $C^{+};Pten^{L/L};K\text{-}ras^{L/W}$ sphere cells appeared morbid with poorly differentiated carcinoma (Fig 6A, left panel). Extensive micro- and macro-metastases was observed in the lymph nodes, lung, and liver of mice received $C^{+};Pten^{L/L};K\text{-}ras^{L/W}$ sphere cells. The metastatic lesions maintained morphology similar to the primary cancers (data not shown). Importantly, recipients of either $C^{+};K\text{-}ras^{L/W}$ or $C^{+};Pten^{L/L}$ sphere cell transplants revealed no detectable macrometastasis or morbidity by 10 wks post-transplantation (data not shown), suggesting that concomitant alteration of both PTEN/PI3K and RAS/MAPK pathways in stem/progenitor cells is required for the metastasis development in the orthotopic transplantation models.

To further support our hypothesis that stem/progenitor cells can reconstitute both EMT and metastatic phenotypes, we FACS sorted the LSC^{high}, LSC^{low} and $Epcam^{low}/CD24^{low}$ mesenchymal subpopulations from $C^{+};K\text{-}ras^{L/W}$, $C^{+};Pten^{L/L}$ and $C^{+};Pten^{L/L};K\text{-}ras^{L/W}$ mutant prostates at age of 8-10 wks (Supplemental Fig. 7B and data not shown), followed by orthotopic transplantation. Consistent with our previous studies, transplantation of *Pten*-null LSC^{high} cells could form adenocarcinoma (Fig 6A, right panel) (26) but without detectable metastasis. However, in the recipients of $C^{+};Pten^{L/L};K\text{-}ras^{L/W}$ LSC^{high} cells and $Epcam^{low}/CD24^{low}$ mesenchymal cells, we observed similar EMT and metastatic phenotypes (Fig.

6B). PCR genotyping of resected metastatic lesions validated the presence of $C^{+};Pten^{-/-};K\text{-}ras^{G12D/W}$ cancer cells (Supplemental Fig. 7C). Therefore, both LSC^{high} and $Epcam^{low}/CD24^{low}$ stem/progenitor cells isolated from $C^{+};Pten^{L/L};K\text{-}ras^{L/W}$ mutant mice have enhanced prostate capacity to reconstitute EMT and drive distant metastasis compared to stem/progenitor cells with either PI3K activation or RAS/MAPK activation alone.

Pharmacological targeting of RAS/MAPK signaling inhibits metastatic disease initiated from stem/progenitor cells

Since transplantation of stem/progenitor cells isolated from $C^{+};Pten^{L/L};K\text{-}ras^{L/W}$ mutants yielded metastatic disease with reliable kinetics, we investigated whether targeting of the PI3K/AKT and RAS/MAPK signaling pathways could inhibit such a phenotype. In order to non-invasively monitor metastasis in vivo, we crossed the *Rosa26-Luc* reporter line onto the compound mutant mice so both primary and metastatic lesions can be easily monitored via bioluminescence imaging (BLI) (Fig 7A and data not shown). We first tested the ability of mTOR inhibitor rapamycin (4 mg/kg/d, I.P.) and MEK inhibitor PD325901 (5 mg/kg/d, P.O.) to effectively inhibit the PI3K and RAS pathways in vivo, using $C^{+};Pten^{L/L};K\text{-}ras^{L/W}$ mutant mice. As shown in Fig 7B, left panels, these small molecule inhibitors could hit their respective pathways in vivo, indicated by the reduction of their downstream surrogate markers P-S6 and P-MAPK staining. Coinciding with efficient reduction of phospho-targets, we observed marked reduction of Ki67+ cells in $C^{+};Pten^{L/L};K\text{-}ras^{L/W}$ mutants treated with rapamycin and PD325901 (Fig 7B, middle panel).

NOD;SCID;IL2rγ-null male mice were then orthotopically transplanted with approximately 2×10^{3} sphere cells derived from $C^{+};Pten^{L/L};K\text{-}ras^{L/W}$;*Rosa26-luc* mice. Two days post-injection, mice were treated daily with placebo, rapamycin and/or, PD325901 and tumor growth and metastasis were monitored by weekly *in vivo* BLI. While placebo treated mice showed rapid primary disease and progression to lung metastasis, as indicated by BLI signals (Fig. 7C, left panel; n=10), mice receiving combination treatment demonstrated both reduced primary tumor burden and little detectable signal in the thoracic region (Fig. 7C; left panel and quantified in middle panel; n=10). Histological analysis revealed that combination treatment significantly abolished enhanced cell proliferation and EMT phenotype seen in placebo cohort of sphere transplantation recipients (Fig. 7B; middle and right panels) and the metastatic potential of the $C^{+};Pten^{L/L};K\text{-}ras^{L/W}$;*Rosa26-luc* sphere cells to the lung (Fig. 7C; right panel). To further test our hypothesis that RAS/MAPK pathway activation is critical for the promotion of metastatic disease, we treated transplantation recipients with only the MEK inhibitor. After 3-4 weeks of daily treatment with PD325901, we observed a similar reduction in metastasis (Fig. 7C; n=10) although the effect on primary cancers were less significant compared to combination treatment. Together these data suggest that the RAS/MAPK pathway activation, in collaboration with PTEN loss or PI3K pathway activation, indeed, plays an essential role in the development of metastatic prostate cancers and that co-targeting both pathways may be effective in preventing metastasis or slow down tumor progression.

DISCUSSION

The study of molecular mechanisms underlying late stage metastatic prostate cancer has been challenging partly as a result of the paucity of prostate cancer models that recapitulate the multistep process of the metastasis. While alterations in the PTEN/PI3K/AKT signaling axis occurs frequently in human disease, such pathway alterations are not sufficient to manifest a significant metastatic phenotype in preclinical animal models (3) (4) (5) (38). In this study, we identified significant enhancement of RAS signaling in both recurrent primary tumors and bone metastasis. In consideration of these findings, we evaluated the possibility that RAS/MAPK activation could serve as a critical, additional hit to alteration of PTEN/

PI3K/AKT signaling in promoting prostate cancer progression and metastasis (Fig. 7D). Through coordinate *Pten* deletion and *K-ras*$^{G12D/W}$ activation, we observed markedly enhanced tumor progression compared to *Pten* deletion alone. Striking features of *C*$^{+}$*;Pten*$^{L/L}$*;K-ras*$^{L/W}$ and *C*$^{+}$*;Pten*$^{L/W}$*;K-ras*$^{L/W}$ mutants included the presence of EMT and significant metastatic burden. Importantly, our study also demonstrated that both LSC^{high} epithelial and Epcam^{low}/CD24^{low} mesenchymal stem/progenitor cells have sphere forming activity *in vitro* and could reconstitute both local invasive and distance metastatic disease *in vivo*.

EMT has been postulated to play a critical role in the process of metastasis (39) (40) (41). Expression of EMT markers is correlated with human prostate cancer progression as exemplified by the enhanced levels of the Twist (36) and N-cadherin (19) in late stage primary and metastatic diseases. Moreover, monoclonal antibody targeting of N-cadherin significantly delays progression in prostate cancer xenograft models (19). However, since few preclinical prostate cancer models progress from invasive carcinoma to EMT and metastasis, the functional significance and the pathways involved with EMT have been difficult to study. Using the *Pten*;p53 prostate cancer model (6), a recent study derived lineage specific cell lines which could metastasize upon orthotopic injection into immune compromised hosts (7). However, the interpretation of these findings is confounded by the fact that primary *Pten*;p53 mutant tumors rarely show extensive metastasis and that derived cell lines may undergo in vitro adaptation or acquire additional mutations. Therefore, the new *Pten*-null;*K-ras* activated model provides an unique opportunity for studying the significant impact of EMT in prostate cancer progression in vivo and the pathway that regulates the EMT biology in the context of PTEN loss. Since both K-ras and B-raf alterations occur in primary and metastatic prostate cancer (2), it will be important to model these alterations and determine if these genetic changes have distinct or overlapping roles in prostate cancer development.

Cells with qualities of stemness and invasiveness have also been postulated to confer greater therapeutic resistance, particularly in recurrent disease (42). If true, then such a hypothesis would explain the relatively poor response that therapies have towards metastatic cancers in comparison to differentiated primary tumors. Recent studies using breast cancer cell lines treated with paclitaxel or 5-fluorouracil, showed a 5-fold increase in CD44^{+}/CD24^{low} cells (43) while primary breast cancer samples isolated from chemotherapy treated patients showed a 7-fold increase in the same cell population (44). That the CD44^{+}/CD24^{low} cells share a stem cell signature and mesenchymal characteristics suggests that EMT may involve in the formation of cancer stem cells and therapeutic resistance. In prostate cancer, such studies are far fewer in number; however the CD44^{+}CD24^{low} subpopulation isolated from prostate cancer cell lines has been attributed to both stemness and invasiveness mediated by EMT (45) and correlated with poor clinical outcome in prostate cancer patients (46). In our study, we have identified significant expansion of Epcam^{low}/CD24^{low} mesenchymal cells that have sphere forming activity and can lead to the regeneration of primary and metastatic lesions upon orthotopic transplantation. It will be interesting to test whether this is the population responsible for therapeutic resistance.

Since our model is based on the coordinate loss of *Pten* and Ras activation, we tested the effectiveness of combined mTOR and MEK inhibition on stem/progenitor cell-mediated transplantations. We observed near complete inhibition of metastatic lung lesions in treatment cohorts. Previous studies have demonstrated that combined pharmacological targeting of mTOR and MEK may lead to reduced primary tumor progression (31). Thus, to further test that RAS/MAPK signaling serves a critical step in the metastatic process, we also treated animals with MEK inhibitor alone. Remarkably, using only PD325901, we also observed near complete abolishment of metastasis, possibly as a result of impeding Ras

dependent EMT (Fig 7D). Collectively, our observations indicate that in *Pten*-null;Ras activated prostate cancer the RAS/MAPK pathway plays a significant role in metastasis.

Supplementary Material

Refer to Web version on PubMed Central for supplementary material.

Acknowledgments

We thank We thank Drs. Liang Cheng (Indiana University), Adeboye Osunkoya, (Emory University), Steven Shen (the Methodist Hospital) and Jorge Yao (University of Rochester) for providing de-identified pathologic material of bony metastasis. DJM was supported by NIH F32 CA112988-01 and CIRM TG2-01169; LMT is supported by NIH T32 CA009056. This work has been supported in part by awards from the Prostate Cancer Foundation (to HW and JH), DOD Idea Development Award (to JH) and a grant from NIH (R01 CA107166 and RO1 CA121110 to HW).

REFERENCES

1. ACS. American Cancer Society. Cancer Facts & Figures. 2010
2. Taylor BS, Schultz N, Hieronymus H, et al. Integrative genomic profiling of human prostate cancer. Cancer Cell. 2010; 18:11–22. [PubMed: 20579941]
3. Wang S, Gao J, Lei Q, et al. Prostate-specific deletion of the murine Pten tumor suppressor gene leads to metastatic prostate cancer. Cancer Cell. 2003; 4:209–21. [PubMed: 14522255]
4. Svensson RU, Haverkamp JM, Thedens DR, Cohen MB, Ratliff TL, Henry MD. Slow disease progression in a C57BL/6 pten-deficient mouse model of prostate cancer. Am J Pathol. 2011; 179:502–12. [PubMed: 21703427]
5. Ma X, Ziel-van der Made AC, Autar B, et al. Targeted biallelic inactivation of Pten in the mouse prostate leads to prostate cancer accompanied by increased epithelial cell proliferation but not by reduced apoptosis. Cancer Res. 2005; 65:5730–9. [PubMed: 15994948]
6. Chen Z, Trotman LC, Shaffer D, et al. Crucial role of p53-dependent cellular senescence in suppression of Pten-deficient tumorigenesis. Nature. 2005; 436:725–30. [PubMed: 16079851]
7. Martin P, Liu YN, Pierce R, et al. Prostate Epithelial Pten/TP53 Loss Leads to Transformation of Multipotential Progenitors and Epithelial to Mesenchymal Transition. Am J Pathol. 2011; 179:422–35. [PubMed: 21703421]
8. Kim MJ, Cardiff RD, Desai N, et al. Cooperativity of Nkx3.1 and Pten loss of function in a mouse model of prostate carcinogenesis. Proc Natl Acad Sci U S A. 2002; 99:2884–9. [PubMed: 11854455]
9. Gumerlock PH, Poonamallee UR, Meyers FJ, deVere White RW. Activated ras alleles in human carcinoma of the prostate are rare. Cancer Res. 1991; 51:1632–7. [PubMed: 1998954]
10. Cho NY, Choi M, Kim BH, Cho YM, Moon KC, Kang GH. BRAF and KRAS mutations in prostatic adenocarcinoma. Int J Cancer. 2006; 119:1858–62. [PubMed: 16721785]
11. Carter BS, Epstein JI, Isaacs WB. ras gene mutations in human prostate cancer. Cancer Res. 1990; 50:6830–2. [PubMed: 2208148]
12. Silan F, Gultekin Y, Atik S, et al. Combined point mutations in codon 12 and 13 of KRAS oncogene in prostate carcinomas. Mol Biol Rep. 2011
13. Xiao-Song Wang SS, Dhanasekaran Saravana M. Ateeq Bushra, Sasaki Atsuo T. Jing Xiaojun, Robinson Daniel, Cao Qi, Prensner John R. Yocum Anastasia K. Wang Rui, Fries Daniel F. Han Bo, Asangani Irfan A. Cao Xuhong, Li Yong, Omenn Gilbert S. Pflueger Dorothee, Gopalan Anuradha, Reuter Victor E. Kahoud Emily Rose, Cantley Lewis C. Rubin Mark A. Palanisamy Nallasivam, Varambally Sooryanarayana, Chinnaiyan Arul M. KRas Oncogene Rearrangments and Gene Fusions: Unexpected Rare Encounters in Late-Stage Prostate Cancers. Cancer Discovery. 2011; 1:35–43. [PubMed: 22140652]
14. Bakin RE, Gioeli D, Bissonette EA, Weber MJ. Attenuation of Ras signaling restores androgen sensitivity to hormone-refractory C4-2 prostate cancer cells. Cancer Res. 2003; 63:1975–80. [PubMed: 12702591]

15. Erlich S, Tal-Or P, Liebling R, et al. Ras inhibition results in growth arrest and death of androgen-dependent and androgen-independent prostate cancer cells. Biochem Pharmacol. 2006; 72:427–36. [PubMed: 16780807]
16. Suzuki A, Nakano T, Mak TW, Sasaki T. Portrait of PTEN: messages from mutant mice. Cancer science. 2008; 99:209–13. [PubMed: 18201277]
17. Yin J, Pollock C, Tracy K, et al. Activation of the RalGEF/Ral pathway promotes prostate cancer metastasis to bone. Mol Cell Biol. 2007; 27:7538–50. [PubMed: 17709381]
18. Jackson EL, Willis N, Mercer K, et al. Analysis of lung tumor initiation and progression using conditional expression of oncogenic K-ras. Genes Dev. 2001; 15:3243–8. [PubMed: 11751630]
19. Tanaka H, Kono E, Tran CP, et al. Monoclonal antibody targeting of N-cadherin inhibits prostate cancer growth, metastasis and castration resistance. Nat Med. 2010; 16:1414–20. [PubMed: 21057494]
20. Gregorian C, Nakashima J, Dry SM, et al. PTEN dosage is essential for neurofibroma development and malignant transformation. Proc Natl Acad Sci U S A. 2009; 106:19479–84. [PubMed: 19846776]
21. Guo W, Lasky JL, Chang CJ, et al. Multi-genetic events collaboratively contribute to Pten-null leukaemia stem-cell formation. Nature. 2008; 453:529–33. [PubMed: 18463637]
22. Lapointe J, Li C, Higgins JP, et al. Gene expression profiling identifies clinically relevant subtypes of prostate cancer. Proc Natl Acad Sci U S A. 2004; 101:811–6. [PubMed: 14711987]
23. Plaisier SB, Taschereau R, Wong JA, Graeber TG. Rank-rank hypergeometric overlap: identification of statistically significant overlap between gene-expression signatures. Nucleic Acids Res. 2010; 38:e169. [PubMed: 20660011]
24. Mulholland DJ, Tran LM, Li Y, et al. Cell Autonomous Role of PTEN in Regulating Castration-Resistant Prostate Cancer Growth. Cancer Cell. 2011
25. Soriano P. Generalized lacZ expression with the ROSA26 Cre reporter strain. Nat Genet. 1999; 21:70–1. [PubMed: 9916792]
26. Mulholland DJ, Xin L, Morim A, Lawson D, Witte O, Wu H. Lin-Sca-1+CD49fhigh stem/progenitors are tumor-initiating cells in the Pten-null prostate cancer model. Cancer Res. 2009; 69:8555–62. [PubMed: 19887604]
27. Jiao J, Wang S, Qiao R, et al. Murine cell lines derived from Pten null prostate cancer show the critical role of PTEN in hormone refractory prostate cancer development. Cancer Res. 2007; 67:6083–91. [PubMed: 17616663]
28. Gioeli D, Mandell JW, Petroni GR, Frierson HF Jr. Weber MJ. Activation of mitogen-activated protein kinase associated with prostate cancer progression. Cancer Res. 1999; 59:279–84. [PubMed: 9927031]
29. Jackson EL. Analysis of lung tumor initiation and progression using conditional expression of oncogenic K-ras. Genes Dev. 2001; 15:3243–8. [PubMed: 11751630]
30. Wu X, Wu J, Huang J, et al. Generation of a prostate epithelial cell-specific Cre transgenic mouse model for tissue-specific gene ablation. Mech Dev. 2001; 101:61–9. [PubMed: 11231059]
31. Kinkade CW, Castillo-Martin M, Puzio-Kuter A, et al. Targeting AKT/mTOR and ERK MAPK signaling inhibits hormone-refractory prostate cancer in a preclinical mouse model. J Clin Invest. 2008; 118:3051–64. [PubMed: 18725989]
32. Gioeli D, Wunderlich W, Sebolt-Leopold J, et al. Compensatory pathways induced by MEK inhibition are effective drug targets for combination therapy against castration-resistant prostate cancer. Mol Cancer Ther. 2011; 10:1581–90. [PubMed: 21712477]
33. Bild AH, Yao G, Chang JT, et al. Oncogenic pathway signatures in human cancers as a guide to targeted therapies. Nature. 2006; 439:353–7. [PubMed: 16273092]
34. Chen Z, Zhang C, Wu D, et al. Phospho-MED1-enhanced UBE2C locus looping drives castration-resistant prostate cancer growth. EMBO J. 2011; 30:2405–19. [PubMed: 21556051]
35. Mani SA, Guo W, Liao MJ, et al. The epithelial-mesenchymal transition generates cells with properties of stem cells. Cell. 2008; 133:704–15. [PubMed: 18485877]
36. Kwok WK, Ling MT, Lee TW, et al. Up-regulation of TWIST in prostate cancer and its implication as a therapeutic target. Cancer Res. 2005; 65:5153–62. [PubMed: 15958559]

37. Bastide C, Bagnis C, Mannoni P, Hassoun J, Bladou F. A Nod Scid mouse model to study human prostate cancer. Prostate Cancer Prostatic Dis. 2002; 5:311–5. [PubMed: 12627217]
38. Majumder PK, Yeh JJ, George DJ, et al. Prostate intraepithelial neoplasia induced by prostate restricted Akt activation: the MPAKT model. Proc Natl Acad Sci U S A. 2003; 100:7841–6. [PubMed: 12799464]
39. Maestro R, Dei Tos AP, Hamamori Y, et al. Twist is a potential oncogene that inhibits apoptosis. Genes Dev. 1999; 13:2207–17. [PubMed: 10485844]
40. Vega S, Morales AV, Ocana OH, Valdes F, Fabregat I, Nieto MA. Snail blocks the cell cycle and confers resistance to cell death. Genes Dev. 2004; 18:1131–43. [PubMed: 15155580]
41. Yang J, Mani SA, Donaher JL, et al. Twist, a master regulator of morphogenesis, plays an essential role in tumor metastasis. Cell. 2004; 117:927–39. [PubMed: 15210113]
42. Pardal R, Clarke MF, Morrison SJ. Applying the principles of stem-cell biology to cancer. Nat Rev Cancer. 2003; 3:895–902. [PubMed: 14737120]
43. Fillmore CM, Kuperwasser C. Human breast cancer cell lines contain stem-like cells that self-renew, give rise to phenotypically diverse progeny and survive chemotherapy. Breast Cancer Res. 2008; 10:R25. [PubMed: 18366788]
44. Yu F, Yao H, Zhu P, et al. let-7 regulates self renewal and tumorigenicity of breast cancer cells. Cell. 2007; 131:1109–23. [PubMed: 18083101]
45. Klarmann GJ, Hurt EM, Mathews LA, et al. Invasive prostate cancer cells are tumor initiating cells that have a stem cell-like genomic signature. Clin Exp Metastasis. 2009; 26:433–46. [PubMed: 19221883]
46. Hurt EM, Kawasaki BT, Klarmann GJ, Thomas SB, Farrar WL. CD44+ CD24(−) prostate cells are early cancer progenitor/stem cells that provide a model for patients with poor prognosis. Br J Cancer. 2008; 98:756–65. [PubMed: 18268494]

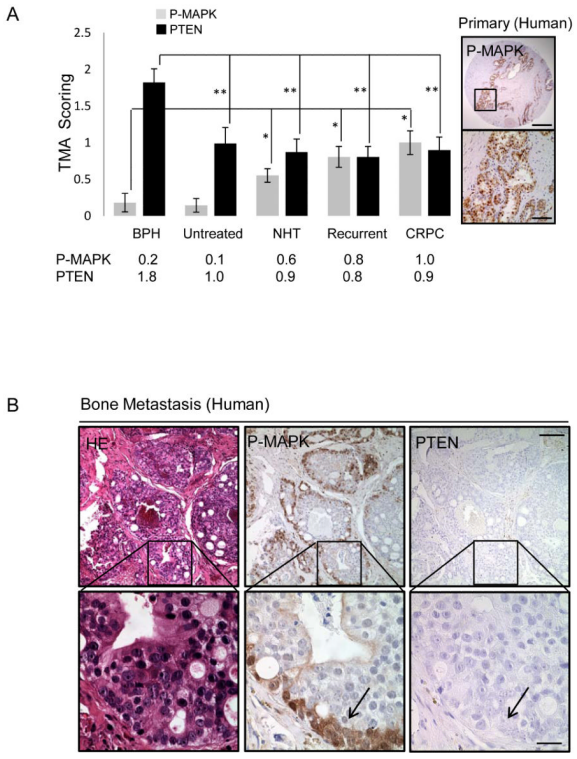

Figure 1. RAS/MAPK signaling is enriched in human prostate cancer

A, PTEN and P-MAPK expression in human TMAs (patient samples = 194, cores = 388) (left) and P-MAPK expression in recurrent Prostate cancer (right), *, $p<0.05$, low mag bar = 1 mm, high mag bar = 100 μm. *B*, Expression of PTEN and P-MAPK in human bone metastasis. low mag bar = 250 μm, high mag bar = 50 μm.

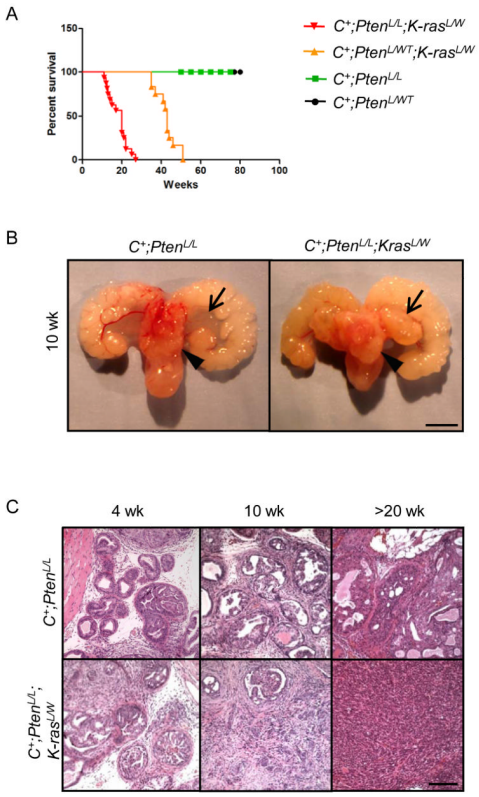

Figure 2. *Pten* loss and Ras activation cooperate to enhance murine prostate cancer progression

A, Kaplan Meier survival curve of *Pten* and *Pten;K-ras* mutants. *B*, Gross structure of intact $C^{+};Pten^{L/L}$ and $C^{+};Pten^{L/L};K\text{-}ras^{L/W}$ mutant prostates at 10 wks (arrow head = lateral lobe, arrow = anterior lobe), bar = 4 mm. *C*, Histology of intact $C^{+};Pten^{L/L}$ and $C^{+};Pten^{L/L};K\text{-}ras^{L/W}$ mutant prostates at 4, 10 and >20 wks, bar = 250 μm.

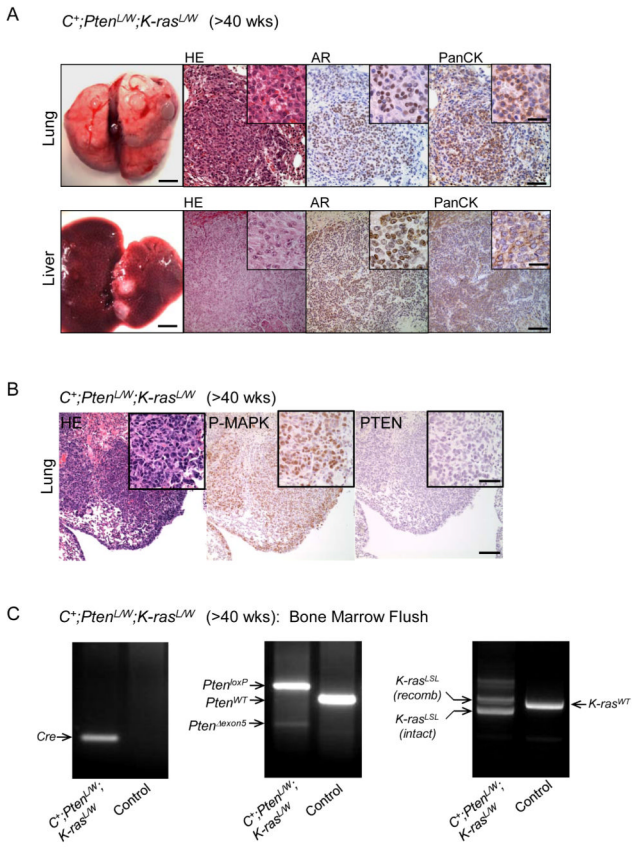

Figure 3. *Pten* loss and Ras activation cooperate to significantly enhance metastatic burden

A, Gross lung and liver structure showing the presence of macrometastasis and corresponding stains for HE, androgen receptor (AR) and pan-cytokeratin (PanCK) in $C^{+};Pten^{L/WT};K\text{-}ras^{L/W}$ mutants (>40 wks). Low mag bar = 150 μm, high mag bar = 50 μm. *B*, Lung lesions from $C^{+};Pten^{L/W};K\text{-}ras^{L/W}$ mutants showing P-MAPK and PTEN expression. Low mag bar = 150 μm, high mag bar = 50 μm. *C*, Bone marrow flush and PCR genotyping for excised *Pten* (Δexon5) and recombined *LSL-K-Ras* in $C^{+};Pten^{L/W};K\text{-}ras^{L/WT}$ and control (*WT*) mice.

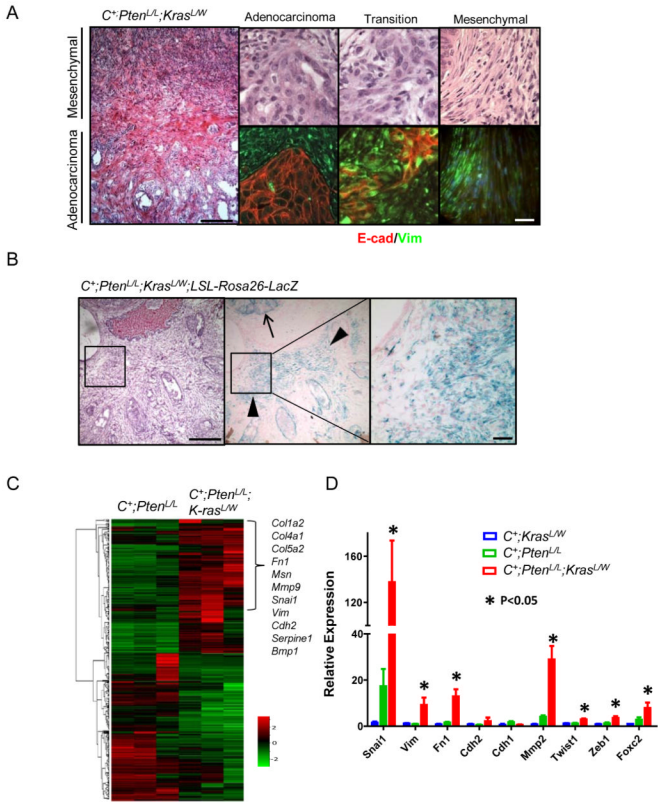

Figure 4. *Pten* loss and Ras pathway activation propagate an EMT signature

A, Histology (left, top) and immunostains (E-cadherin, Vimentin) (bottom) showing regions of transition between epithelial and mesenchymal phenotypes, low mag bar = 500 μm, high mar bar = 100 μm. *B*, Lineage tracing using beta-gal staining and the *LSL-Rosa26-LacZ* reporter in conjunction with the epithelial specific probasin promoter in $C^{+};Pten^{L/L};K\text{-}ras^{L/W}$ mutants (10 wks), low mag bar = 500 μm, high mar bar = 200 μm. *C*, Gene microarray analysis showing EMT pathway gene activity in between $C^{+};Pten^{L/L};K\text{-}ras^{L/W}$ and $C^{+};Pten^{L/L}$ mutants. *D*, RT-PCR confirmation of EMT gene alterations in $C^{+};Pten^{L/L};K\text{-}ras^{L/W}$ mutant prostates (*, $p < 0.05$).

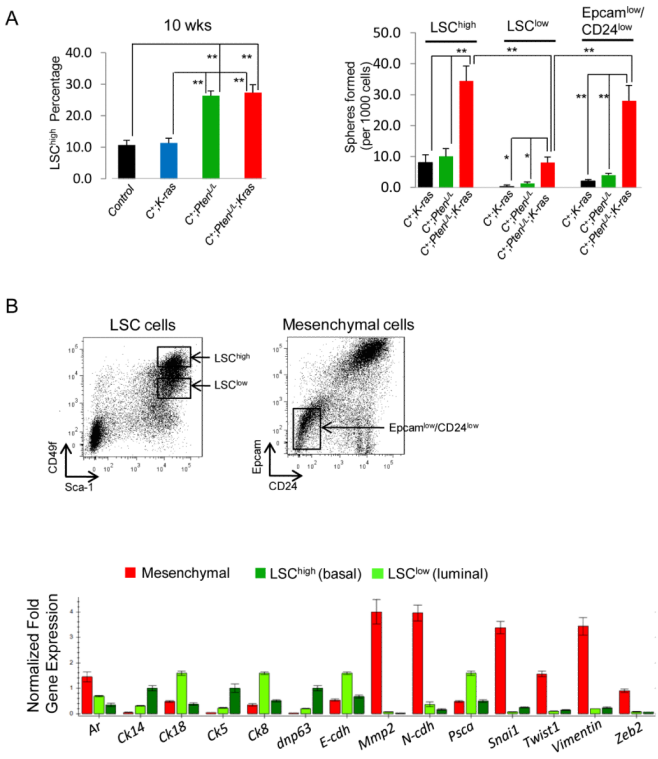

Figure 5. $C^{+};Pten^{L/L};K\text{-}ras^{L/W}$ mutant LSC^{high} and mesenchymal cells show high stem/ progenitor activity

A, Comparison of percentage LSC^{high} subpopulation in control, $C^{+};K\text{-}ras^{L/W}$ $C^{+};Pten^{L/L}$ and $C^{+};Pten^{L/L};K\text{-}ras^{L/W}$ mutant prostates (10 wks) (Left panel). Comparison of sphere plating efficiency between LSC^{high}, LSC^{low} and mesenchymal cells isolated from $C^{+};Pten^{L/L}$ and $C^{+};Pten^{L/L};K\text{-}ras^{L/W}$ mutant prostates (10 wks) (*, $p < 0.05$; **, $p<0.01$) (Right panel). *B*, Isolation of LSC^{high}(Lin^{-}Sca1^{+}CD49f^{high}), LSC^{low} (Lin^{-}Sca1^{+}CD49f^{low}) and mesenchymal cells from $C^{+};Pten^{L/L};K\text{-}ras^{L/W}$ mutants (10 wks) with RT-PCR analysis (lower panel)

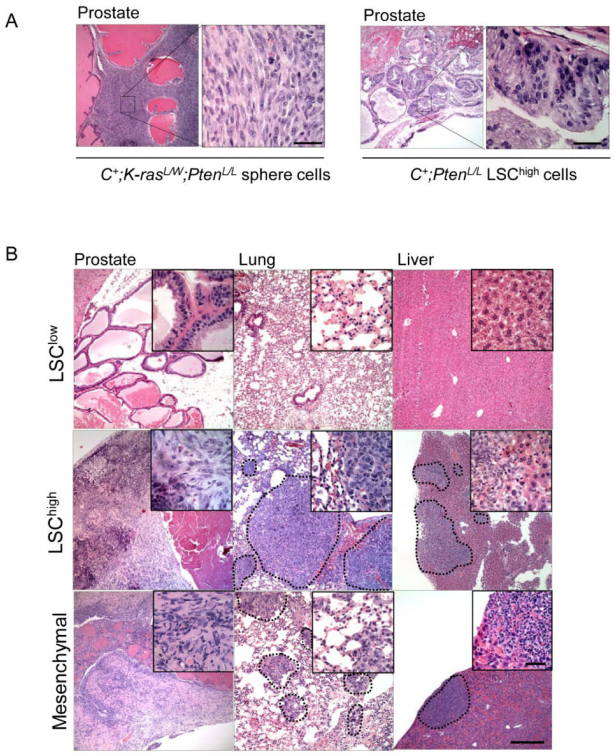

Figure 6. Transplantation of $C^{+};Pten^{L/L};K\text{-}ras^{L/W}$ stem/progenitor cells are sufficient to initiate EMT and metastasis

A, Orthotopic transplantation of $C^{+};Pten^{L/L};K\text{-}ras^{L/W}$ spheres cells (left panel) and $C^{+};Pten^{L/L}$ LSC^{high} cells (right panel) to *NOD;SCID;IL2rγ*-null recipients and resulting pathology (left). *B*, Transplantation of LSC^{low}, LSC^{high} and mesenchymal cells isolated from primary $C^{+};Pten^{L/L};K\text{-}ras^{L/W}$ mutant cells and resulting pathology observed in *NOD;SCID;IL2rγ*-null recipients. Low mag bar = 500 μm, high mag bar = 100 μm.

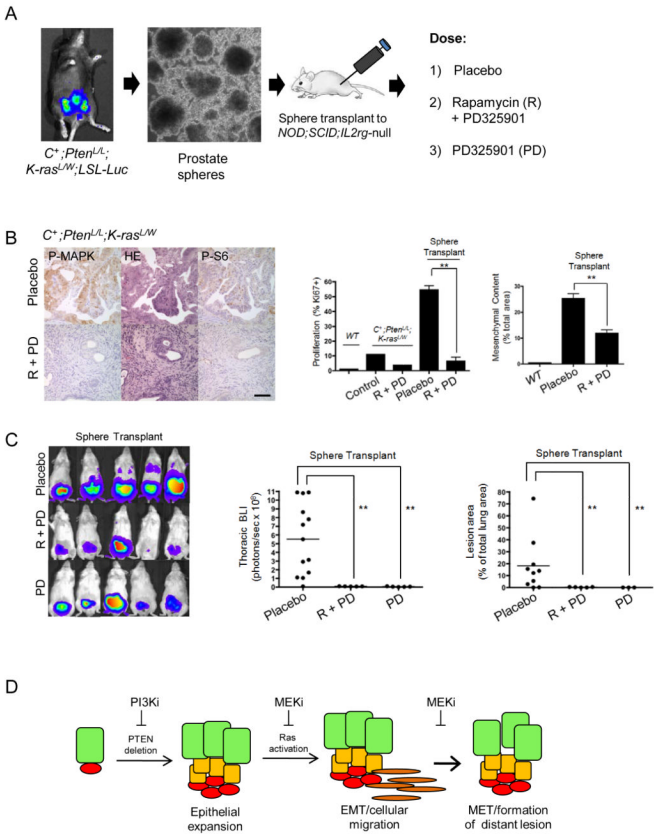

Figure 7. Pharmacological targeting of RAS/MAPK signaling inhibits metastatic disease initiated from $C^{+};Pten^{L/L};K\text{-}ras^{L/W}$ mutant stem/progenitor cells

A, Isolation of prostate sphere cells from $C^{+};Pten^{L/L};K\text{-}ras^{L/W};LSL\text{-}Luc$ mutants and orthotopic injection to *NOD;SCID;IL2rγ*-null mice. Recipients were then treated with either placebo, rapamycin (R) + PD325901 (PD) or PD325901, alone. *B*, Effect of rapamycin/PD325901 treatment on P-MAPK and P-S6 levels (left panel), cell proliferation (Ki67+ index; middle panel) and mesenchymal content (right panel). *C*, Effect of rapamycin/PD325901 or PD325901 on thoracic region BLI (left, middle panels) and metastatic lung lesion content (right panel). *D*, Model showing that Pten-null LSC^{high} cells can initiate prostate cancer and with RAS/MAPK activation lead to EMT, metastatic disease and formation of macrometastatic lesions.